

## Faint AGNs Favor Unexpectedly Long Inter-band Time Lags

TING LI,<sup>1</sup> MOUYUAN SUN,<sup>1</sup> XIAOYU XU,<sup>1</sup> W. N. BRANDT,<sup>2,3,4</sup> JONATHAN R. TRUMP,<sup>5</sup> ZHEFU YU,<sup>6</sup> JUNXIAN WANG,<sup>7,8</sup>  
YONGQUAN XUE,<sup>7,8</sup> ZHENYI CAI,<sup>7,8</sup> WEI-MIN GU,<sup>1</sup> Y. HOMAYOUNI,<sup>5</sup> TONG LIU,<sup>1</sup> JUN-FENG WANG,<sup>1</sup> ZHIXIANG ZHANG,<sup>1</sup> AND  
HAI-KUN LI<sup>1</sup>

<sup>1</sup>*Department of Astronomy, Xiamen University, Xiamen, Fujian 361005, China; msun88@xmu.edu.cn*

<sup>2</sup>*Department of Astronomy & Astrophysics, 525 Davey Lab, The Pennsylvania State University, University Park, PA 16802, USA*

<sup>3</sup>*Institute for Gravitation and the Cosmos, The Pennsylvania State University, University Park, PA 16802, USA*

<sup>4</sup>*Department of Physics, 104 Davey Lab, The Pennsylvania State University, University Park, PA 16802, USA*

<sup>5</sup>*Department of Physics, University of Connecticut, Storrs, CT 06269, USA*

<sup>6</sup>*Department of Astronomy, The Ohio State University, Columbus, OH 43210, USA*

<sup>7</sup>*CAS Key Laboratory for Research in Galaxies and Cosmology, Department of Astronomy, University of Science and Technology of China, Hefei 230026, China*

<sup>8</sup>*School of Astronomy and Space Science, University of Science and Technology of China, Hefei 230026, China*

### ABSTRACT

Inconsistent conclusions are obtained from recent active galactic nuclei (AGNs) accretion disk inter-band time-lag measurements. While some works show that the measured time lags are significantly larger (by a factor of  $\sim 3$ ) than the theoretical predictions of the Shakura & Sunyaev disk (SSD) model, others find that the time-lag measurements are consistent with (or only slightly larger than) that of the SSD model. These conflicting observational results might be symptoms of our poor understanding of AGN accretion physics. Here we show that sources with larger-than-expected time lags tend to be less-luminous AGNs. Such a dependence is unexpected if the inter-band time lags are attributed to the light-travel-time delay of the illuminating variable X-ray photons to the static SSD. If, instead, the measured inter-band lags are related not only to the static SSD but also to the outer broad emission-line regions (BLRs; e.g., the blended broad emission lines and/or diffuse continua), our result indicates that the contribution of the non-disk BLR to the observed UV/optical continuum decreases with increasing luminosity ( $L$ ), i.e., an anti-correlation resembling the well-known Baldwin effect. Alternatively, we argue that the observed dependence might be a result of coherent disk thermal fluctuations as the relevant thermal timescale,  $\tau_{\text{TH}} \propto L^{0.5}$ . With future accurate measurements of inter-band time lags, the above two scenarios can be distinguished by inspecting the dependence of inter-band time lags upon either the BLR components in the variable spectra or the timescales.

*Keywords:* accretion, accretion disks—galaxies: active—quasars: general—quasars: supermassive black holes

### 1. INTRODUCTION

Active Galactic Nucleus (AGN) continua at various UV/optical bands vary coherently, and the long-wavelength emission usually lags the short-wavelength emission with time delays of days. Such short time delays are unexpected in the static Shakura & Sunyaev disk (SSD; Shakura & Sunyaev 1973) model as the relevant radial propagation timescale (i.e., the viscous timescale) is hundreds to thousands of years. Instead, the inter-band cross correlations and time lags ( $\tau$ ) are often understood in the framework of X-ray reprocessing (e.g., Krolik et al. 1991). In this scenario, the central compact X-ray corona can illuminate the disk surface and the absorbed X-ray emission is thermalized and reprocessed as UV/optical emission. The inter-band time lags account for

the differences in the light-travel timescales from the corona to the emission regions of various UV/optical wavelengths.

Recent high-cadence multi-band observations of several Seyfert 1 AGNs suggest that the measured inter-band time lags are longer than the predictions of the X-ray reprocessing of a static SSD by a factor of 2 – 3 (e.g., Fausnaugh et al. 2016; Cackett et al. 2018; McHardy et al. 2018; Edelson et al. 2019). This result is further supported by Pan-STARRS observations (Jiang et al. 2017), which might, however, suffer from significant selection bias (see Appendix A of Homayouni et al. 2019). Possible explanations involve alternative reprocessors, e.g., SSDs with powerful winds which have flatter disk temperature profiles (Li et al. 2019; Sun et al. 2019), SSDs with non-blackbody disk emission (Hall et al. 2018), inhomogeneous SSDs with global temperature fluctuations (Cai et al. 2020; Sun et al. 2020a), or non-disk UV/optical continuum emission from the more extended broad-line clouds (Cackett et al. 2018; Lawther et al. 2018;

Sun et al. 2018a; Chelouche et al. 2019; Korista & Goad 2019).

In contrast, very recent light-curve studies of distant survey quasars (which in general are more luminous than the targeted studies of nearby Seyfert 1 AGNs) from the Dark Energy Survey (DES; e.g., Flaugher et al. 2015)-Australian DES (OzDES; e.g., Lidman et al. 2020) reverberation mapping project (Yu et al. 2020), the Sloan Digital Sky Survey Reverberation Mapping (SDSS-RM) project (Homayouni et al. 2019) and the quasar PG 2308+098 (Kokubo 2018) suggest that the measured inter-band time lags are actually consistent with (or only slightly larger than) the predictions of the X-ray reprocessing of a static SSD.

Microlensing observations of quasars find oversized disks (Morgan et al. 2018), which are actually inconsistent with the time-lag observations of quasars with similar luminosities but agree with the time lags of fainter nearby Seyfert 1 AGNs.

These apparently conflicting observational results might be symptoms of our poor understanding of AGN accretion physics. Meanwhile, Tie & Kochanek (2018) point out that the accretion-disk size induced microlensing time lags add significant systematic uncertainties to gravitational-lensing time delay cosmology. Hence, determining the real accretion-disk sizes are vital for our understanding of AGN central-engine physics and measuring cosmological parameters via gravitational lensing of distant quasars.

Here, we collect a large set of inter-band time-lag measurements from different previously published studies to demonstrate that the ratios of the measured time lags to the expectations of the SSD model anti-correlate with AGN luminosity ( $L$ ). That is, faint AGNs tend to have larger-than-expected inter-band time lags. This result is unexpected in the X-ray reprocessing of a static SSD (hereafter the lamp-post SSD model) and might provide critical clues to the AGN disk-size problem.

## 2. THE MEASURED AND PREDICTED AGN ACCRETION-DISK SIZES

We use the inter-band time lags reported in previous studies to estimate the  $\lambda = 2500 \text{ \AA}$  time lags (hereafter  $\tau_{\text{obs}}$ ); the estimation procedures are presented in Appendix A. Our sample consists of the available local AGNs listed in Table 1 and more distant quasars from DES standard star fields (Yu et al. 2020, hereafter Y20), SDSS-RM (Homayouni et al. 2019, hereafter H19) and PG 2308+098 (Kokubo 2018). We exclude the data from Jiang et al. (2017) and Mudd et al. (2018) as their relevant cadences are sparser than for H19 or Y20 and thus the time lags are likely biased to larger values.

As a second step, we use the estimated black hole mass ( $M_{\text{BH}}$ ) and AGN bolometric luminosity ( $L$ ) to calculate the expected  $\lambda = 2500 \text{ \AA}$  static SSD lag (hereafter  $\tau_{\text{SSD}}$ ; see Eq. 7 of Fausnaugh et al. 2018),

$$\tau_{\text{SSD}} = 0.128X \left( \frac{M_{\text{BH}}}{10^8 M_{\odot}} \right)^{2/3} \left( \frac{f_{\text{Edd}}}{0.1} \right)^{1/3} \text{ days}, \quad (1)$$

where  $f_{\text{Edd}}$  is the ratio of  $L$  to the Eddington luminosity. Note that this formula is valid only if the radiative efficiency

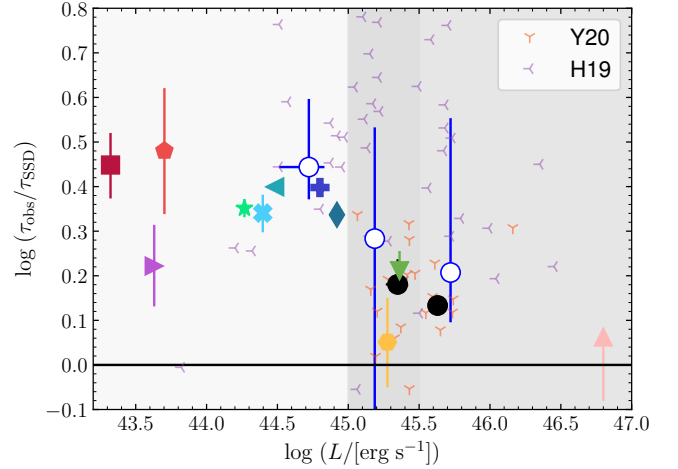


**Figure 1.** The ratio of the observed  $\tau_{\text{obs}}$  to  $\tau_{\text{SSD}}$  anti-correlates with  $L$ . The large colored filled symbols with error bars represent (from the lowest to highest luminosities) NGC 4593, NGC 2617, NGC 4151, Mrk 142, MCG+08-11-011, NGC 5548, NGC 7469, Fairall 9, Ark 120, Mrk 509 and PG 2308+098, respectively; these sources usually have high-cadence and continuous multi-wavelength observations. The small yellow and purple symbols indicate the medians of the quasar time lags from the DES (i.e., Y20) and SDSS-RM (i.e., H19) surveys (while all H19 sources are taken into account in the medians and all subsequent analysis, some H19 sources with negative, extremely small or large ratios are not presented in this figure for the sake of clarity). The H19 sources are divided into three luminosity bins (i.e.,  $\log(L/[\text{erg s}^{-1}]) < 45$ ,  $45 < \log(L/[\text{erg s}^{-1}]) < 45.5$  and  $\log(L/[\text{erg s}^{-1}]) > 45.5$ , respectively; see also the shaded gray regions) and the three bins have similar source numbers; the DES AGNs are divided into two luminosity bins ( $\log(L/[\text{erg s}^{-1}]) < 45.5$  and  $\log(L/[\text{erg s}^{-1}]) > 45.5$ , respectively). The blue open and black filled circles with error bars represent the median ratios for these luminosity bins and their  $1\sigma$  uncertainties (estimated via bootstrapping; the error bars of the black filled circles are too small to show).

is  $\eta = 0.1$ ;  $L$  is estimated from the continuum luminosities at rest-frame  $1350 \text{ \AA}$ ,  $3000 \text{ \AA}$ , or  $5100 \text{ \AA}$  (depending on redshift) with the bolometric corrections recommended by Richards et al. (2006). The factor  $X$  is chosen to be 5.04; that is,  $\tau_{\text{SSD}}$  corresponds to the average time lag of the variable flux (Tie & Kochanek 2018) and is 1.5 times larger than the flux-weighted light-travel time lag adopted in some previous studies (e.g., Fausnaugh et al. 2016). In the third step, the ratio ( $\tau_{\text{diff}}$ ) of the measured  $\tau_{\text{obs}}$  to  $\tau_{\text{SSD}}$  is obtained.

We find that  $\tau_{\text{diff}}$  anti-correlates with  $L$  (see Figure 1), with a Spearman correlation coefficient  $\rho_{\text{spearman,obs}} = -0.78$

(the corresponding  $p$ -value is  $3 \times 10^{-4}$ ).<sup>1</sup> We also confirm that  $\tau_{\text{diff}}$  anti-correlates with  $M_{\text{BH}}$  (the Spearman coefficient and the  $p$ -value are  $-0.69$  and  $4 \times 10^{-3}$ , respectively); however, the partial correlation between  $\tau_{\text{diff}}$  and  $M_{\text{BH}}$  is insignificant once  $L$  is controlled (the Spearman partial-correlation coefficient, which is calculating via the package “ppcor” in R, is  $-0.05$ ). Our results also suggest an apparent disagreement between the microlensing disk-size measurements and the inter-band time-lag observations: the former focus on luminous AGNs but find over-sized disks and the latter suggest that such AGNs have consistent-with-expectation time lags.

To test whether the lamp-post SSD model can explain our results or not, we perform the following experiment. First, we use the measured  $M_{\text{BH}}$  and  $L_{\text{bol}}$  to calculate the static SSD effective temperature ( $T_{\text{eff}}$ ) profile (we again adopt  $\eta = 0.1$ ). Second, we add the additional surface heating due to the X-ray illumination (which is modeled by a damped random-walk process) to obtain the fluctuations of  $T_{\text{eff}}$  and the corresponding mock UV/optical light curves (by integrating the SSD blackbody emission over the whole disk). Note that, the adopted UV/optical bands are the same as real observations. Third, the mock UV/optical inter-band time lags are estimated by utilizing *Javelin* to fit the mock light curves. Fourth, we calculate the corresponding mock time lags at  $2500 \text{ \AA}$  (hereafter  $\tau_{\text{SSD}(\text{sim})}$ ) following the same recipes aforementioned. We repeat this experiment 200 times to account for statistical fluctuations.

The median ratios (and their  $1\sigma$  uncertainties) of  $\tau_{\text{SSD}(\text{sim})}$  to  $\tau_{\text{SSD}}$  (i.e., Eq. 1) are shown in the left panel of Figure 2, which suggests that  $\tau_{\text{SSD}(\text{sim})}$  is on average less than  $\tau_{\text{SSD}}$ ; similar results have been reported by Chan et al. (2020) who therefore propose that the accretion-disk sizes estimated via *Javelin* are underestimates by  $\sim 30\%$  (or 0.15 dex). However, such a bias cannot account for our results. Indeed, the anti-correlation in the left panel of Figure 2 is statistically insignificant (the Spearman coefficient and the  $p$ -value are  $-0.38$  and  $0.14$ , respectively) and much weaker than the observed one. Moreover, a clear anti-correlation between the ratios of  $\tau_{\text{obs}}$  to  $\tau_{\text{SSD}(\text{sim})}$  and  $L$  holds (see the right panel of Figure 2; the Spearman coefficient and the  $p$ -value are  $-0.77$  and  $5 \times 10^{-4}$ , respectively).

### 3. PHYSICAL IMPLICATIONS

Our results are unexpected in the lamp-post SSD model. Some alternative solutions are proposed to account for the AGN disk-size problem. Below, we discuss the physical implications of our results for these models.

#### 3.1. Implications for the X-ray reprocessing models

One model to explain the larger-than-expected time lags for Seyfert AGNs involves disk-atmosphere radiative transfer effects (Hall et al. 2018). If so, our results suggest that the atmosphere effects are weaker in more luminous AGNs. It is unclear what mechanisms can drive this behavior.

Alternatively, Sun et al. (2019) (also see Li et al. 2019) consider SSDs with powerful winds and find that such disks can have larger apparent sizes than the no-wind SSDs. Then, our results indicate that the disk-wind strength should decrease with increasing  $L$ , contradicting observations that luminous AGNs generally have stronger disk winds than their faint counterparts (e.g., Laor & Brandt 2002; Ganguly et al. 2007). Therefore, it seems that the lamp-post wind SSD is not the general solution to the disk-size problems of AGNs with various luminosities although winds might still play an important role in luminous AGNs (see Section 4).

The discrepancy between the observed UV/optical time lags and the lamp-post SSD ones might also be reconciled by increasing the corona scale height to  $\gtrsim 20$  Schwarzschild radii (Kammoun et al. 2021), which effectively enlarges the light travel time. To explain our results, the corona height must then anti-correlate with luminosity.

Instead, several works (Cackett et al. 2018; Lawther et al. 2018; Sun et al. 2018a; Chelouche et al. 2019; Korista & Goad 2019) propose that the diffuse nebular emission from the more distant broad-line region (BLR) clouds also acting as a reprocessor can produce non-disk UV/optical continuum light curves; then, the measured time lags are superpositions of the disk and BLR light-travel time delays and are thus longer than the SSD expectations. This BLR model might explain our results if its contribution to the UV/optical continuum emission anti-correlates with  $L$ . There is a well-known anti-correlation between broad-line strength and  $L$ , a.k.a., the Baldwin effect (Baldwin 1977), and this would imply that less-luminous AGNs similarly have stronger diffuse nebular emission from the BLR. In other words, faint AGNs tend to have larger ratios of the observed to SSD model time lags. We stress that detailed BLR calculations should be performed to quantitatively test this model against our results because the slope of the Baldwin effect for various lines are generally not steep (i.e., the line equivalent width  $\propto L^{-\gamma}$  with  $\gamma \sim 0.1$ ; see, e.g., Shields 2007). Such calculations are beyond the scope of this work; the BLR diffuse nebular emission models, e.g., Korista & Goad (2019), might be expanded to search for such an effect.

We point out that these X-ray reprocessing models cannot simultaneously explain several other aspects of AGN UV/optical variability, e.g., the timescale-dependent color variations (i.e., the lamp-post SSD can explain the variable spectra, but cannot account for the fact that the color variations are timescale dependent; see, e.g., Zhu et al. 2018) and the anti-correlations between variability amplitude and  $L$  (e.g., MacLeod et al. 2010; Sun et al. 2018b). Below, we discuss the alternative disk-corona magnetic coupling scenario (Sun et al. 2020a), which has shown to be successful in repro-

<sup>1</sup> We use the local-AGN measurements and the median values of the sources from H19 and Y20 to calculate the Spearman coefficient unless otherwise specified. This is because, comparing with local AGN measurements, the results of H19 and Y20 have larger uncertainties; thus, we decide to use their median values. Nevertheless, we also calculate the corresponding Spearman coefficient by treating the local AGNs and the quasars from H19 and Y20 equally and find that the coefficient and the  $p$ -value are  $-0.29$  and  $3 \times 10^{-3}$ , respectively; that is, the anti-correlation still exists.

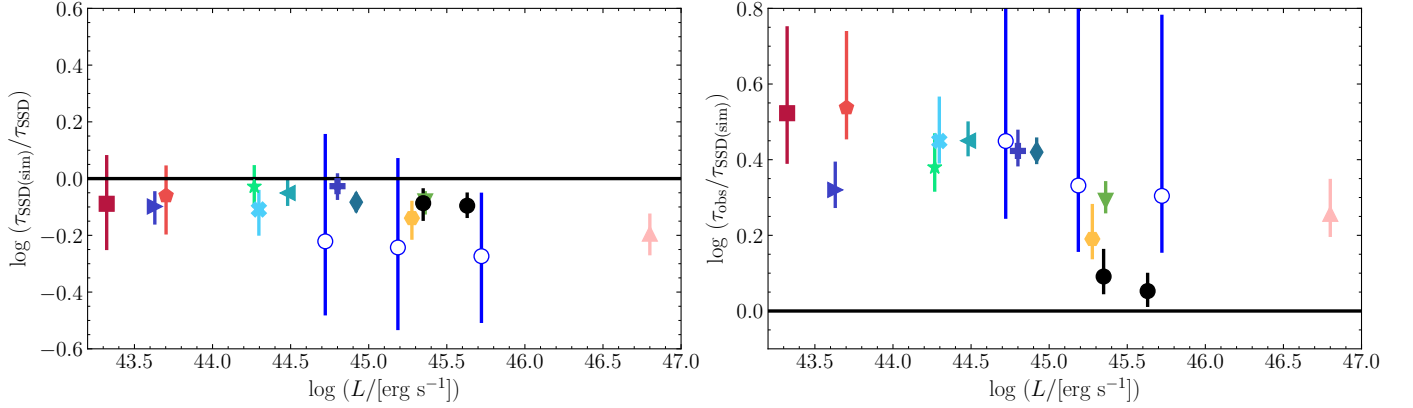


**Figure 2.** Left-panel: the ratio of  $\tau_{\text{SSD}(\text{sim})}$  (i.e., obtained by applying *Javelin* to analysis the lamp-post SSD simulations that mimic real observations) to  $\tau_{\text{SSD}}$  (i.e., Eq. 1) versus  $L$ . Right-panel: the ratio of  $\tau_{\text{obs}}$  to  $\tau_{\text{SSD}(\text{sim})}$  versus  $L$ . The symbols share the same meanings as in Figure 1. The lamp-post SSD model cannot explain our results.

ducing the color variations and the dependences of the variability amplitude upon  $L$  (Sun et al. 2020b), to understand our results in Figure 1.

### 3.2. Implications for the MHD accretion physics

Theoretically speaking, disk temperatures ( $T$ ) should vary in response to the time-dependent magnetohydrodynamic (MHD) turbulent heating with a response on the thermal timescale ( $\tau_{\text{TH}}$ ). For an SSD,  $\tau_{\text{TH}} \sim \alpha^{-1}(GM_{\text{BH}}R^{-3})^{-1/2}$ , where  $\alpha$ ,  $G$ , and  $R$  are the dimensionless viscosity parameter, the gravitational constant, and the distance to the central black hole, respectively. Therefore, the short-wavelength emission which is produced by the inner hotter plasma has a smaller response thermal timescale than the long-wavelength emission. The differences in the response thermal timescale would add an additional inter-band time lag ( $\tau_{\text{add}}$ ), beyond the light-travel time lags. On short timescales ( $t_{\text{dur}}$ ), the observed UV/optical variations are mainly produced in the similar small- $R$  regions with  $\tau_{\text{TH}} \leq t_{\text{dur}}$  as the gas in these regions can vary its temperature significantly, and  $\tau_{\text{add}}$  is small and negligible. And vice versa. For an SSD, at the characteristic radius  $R_{\lambda}$  (with  $k_{\text{B}}T(R_{\lambda}) = hc/\lambda$ , where  $k_{\text{B}}$  and  $h$  are the Boltzmann and Planck constants, respectively; and  $T(R_{\lambda}) \propto (M_{\text{BH}}\dot{M})^{1/4}R_{\lambda}^{-3/4}$ ),  $\tau_{\text{TH}}(R_{\lambda})$  scales as  $\alpha^{-1}L^{0.5}\lambda^2$ . Therefore,  $\tau_{\text{add}}$  would only be prominent for AGNs with small  $L$  (i.e., short  $\tau_{\text{TH}}(R_{\lambda})$ ) or large  $t_{\text{dur}}$ . Below, we consider a specific thermal-fluctuation model to qualitatively reproduce the observed result.

In earlier work, we proposed the corona-heated accretion-disk reprocessing model (hereafter the CHAR model) by assuming the accretion disk and the extremely compact X-ray corona are magnetically coupled (Sun et al. 2020a). Magnetic fluctuations in the corona can alter the disk surface magnetic field, drive variations in the disk MHD turbulent dissipation, and eventually induce coherent multi-band variations. We have predicted that  $\tau_{\text{dif}}$  increases with decreasing  $L$  for sources with similar monitoring durations (see Figures 8 & 16 of Sun et al. 2020a).

The first two model parameters,  $M_{\text{BH}}$  and  $\dot{M}$ , are fixed according to the observational constraints. The only free parameter  $\alpha$  might be 0.1 – 0.4 according to studies of the outbursts of dwarf nova or soft X-ray transients (e.g., King et al. 2007). We fix<sup>2</sup>  $\alpha = 0.1$  and obtain the mock multi-wavelength light curves by considering the CHAR model for all sources in Figure 1. The mock inter-band time lags are measured by again adopting *Javelin*. The ratios (hereafter  $\tau_{\text{diff, mock}}$ ) of the CHAR time lags (hereafter  $\tau_{\text{CHAR}}$ ) and  $\tau_{\text{SSD}}$  are calculated following the same recipes aforementioned. Indeed,  $\tau_{\text{diff, mock}}$  also anti-correlates with  $L$  (see the left panel of Figure 3). Moreover, the ratios of  $\tau_{\text{CHAR}}$  to  $\tau_{\text{obs}}$  show a lack of dependence upon  $L$  (see the right panel of Figure 3), i.e., the CHAR model can explain our results.

For an AGN, our CHAR model also predicts that the inter-band time lags of the slow variations are longer than those of the fast variations (see Figure 7 of Sun et al. 2020a). Recently, instead of simply measuring the inter-band time lags of NGC 7469 (which is considered in Figure 1), Pahari et al. (2020) further split the 1825 Å and 1315 Å light curves into slow (i.e., timescale > 5 days) and fast (timescale < 5 days) variations and find that the corresponding time lags are  $0.29 \pm 0.06$  days and  $0.04 \pm 0.12$  days, respectively. We fix the two CHAR model parameters,  $M_{\text{BH}}$  and  $L$ , according to the NGC 7469 observations and  $\alpha = 0.1$  to generate the mock light curves. The mock light curves are also split into slow and fast components following the methodology of Pahari et al. (2020). The resulting lag for the slow (fast) variation component is  $0.27 \pm 0.2$  days ( $0.04 \pm 0.03$  days) which agrees with the results by Pahari et al. (2020). The anti-correlation between the time lag and the timescale might also be responsible for the fact that NGC 4593 and NGC 4151 do not seem to follow the anti-correlation found in Figure 1. Indeed, while NGC 4593 and NGC 4151 have the lowest luminosities, their size ratios are not the largest.

<sup>2</sup> Note that the CHAR model with  $\alpha \simeq 0.2$  can also explain the results.

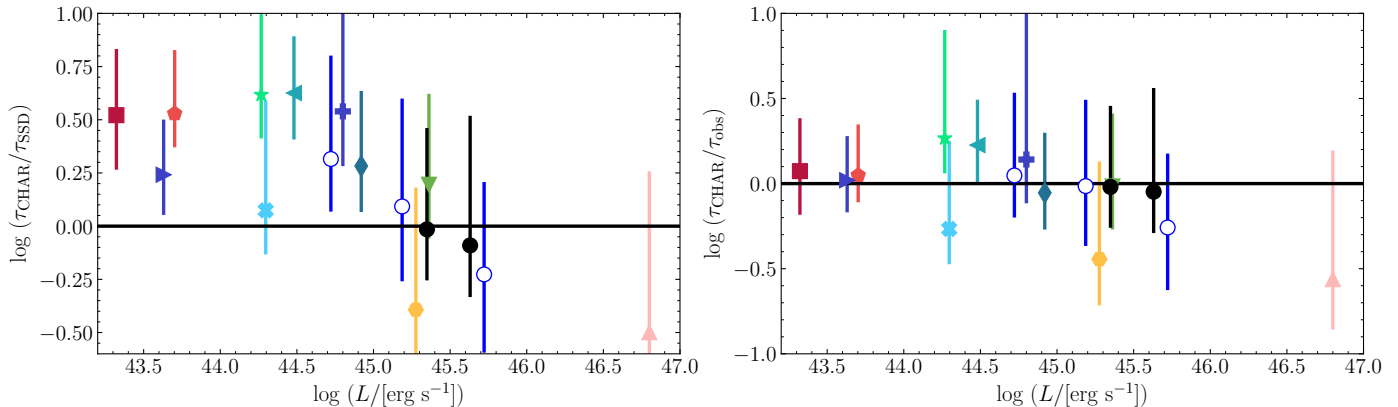


**Figure 3.** Left-panel: the ratio of  $\tau_{\text{CHAR}}$  to  $\tau_{\text{SSD}}$  (i.e., Eq. 1) versus  $L$ . Right-panel: the ratio of  $\tau_{\text{CHAR}}$  to  $\tau_{\text{obs}}$  versus  $L$ . The symbols share the same meanings as in Figure 1. The CHAR model (on average) successfully accounts for the observed inter-band time lags.

We speculate that this is because their monitoring time durations are relatively short ( $\lesssim 60$  days).

#### 4. COMPARING WITH MICROLENSING OBSERVATIONS

Our results in Figure 1 suggest that microlensing observations of quasars (which often find larger-than-expected disk sizes) are, in fact, inconsistent with the time-lag observations of quasars with similar luminosities. Note that the inter-band time lags of a gravitationally lensed AGN 0957+561 were obtained by [Gil-Merino et al. \(2012\)](#). By interpreting the time lags as the variability-weighted ones (i.e., Eq. 1 with  $X = 5.04$ ), we use their UV/optical measurements and the methodology aforementioned to obtain the corresponding  $r$ -band half-light radius (i.e.,  $\log(r_{\text{half}}(r)/\text{cm}) = 15.82$ ). Recently, [Cornachione et al. \(2020\)](#) obtained its microlensing  $\log(r_{\text{half}}(r)/\text{cm}) = 16.66^{+0.37}_{-0.62}$ . The difference of the two results is 0.84 dex albeit with a large uncertainty. Hence, any X-ray reprocessing models that actually enlarge the effective disk sizes might not explain this discrepancy.

In our CHAR model, the actual disk sizes are similar to the SSD model. In addition, the median time lag of our CHAR model is considerably smaller than the SSD model (see the left panel of Figure 3). Disk winds are probably common in luminous AGNs (e.g., [Laor & Brandt 2002](#); [Ganguly et al. 2007](#); [Laor & Davis 2014](#)) and can make the actual disk sizes larger than the no-wind SSD model (e.g., [Sun et al. 2019](#)). If we also consider the CHAR model with winds, the predicted median time lag approaches the SSD model and is more consistent with observations. At the same time, the windy CHAR model has a larger half-light radius and can account for the microlensing observations (e.g., [Morgan et al. 2018](#); [Li et al. 2019](#)). In summary, the possible discrepancy between the inter-band time lags and microlensing observations might be a unique probe of winds and corona-disk magnetic coupling. Future inter-band time-lag measurements of gravitationally lensed quasars can verify this idea.

We have collected the inter-band time lags for a large AGN sample. We find tentative evidence that the ratio of the observed to SSD time lags anti-correlates with  $L$ ; this anti-correlation is unexpected in the lamp-post SSD (with or without winds and/or disk-atmosphere scattering) model. Our result indicates that the inter-band time lags are not solely determined by the spatial sizes of the emission regions but contain important information regarding the disk inner thermal fluctuations or the BLR structure. While both the BLR and CHAR models can explain our results, they have entirely different predictions. For the BLR model, we would expect that the time-lag ratios depend upon the BLR components in the variable spectra. For the CHAR model, we suggest that the time lags increase with the variability timescales. Future time-domain surveys such as the Rubin Observatory’s Legacy Survey of Space and Time (e.g., [Ivezić et al. 2019](#)) can measure inter-band time lags for a large number of AGNs with various properties, thereby starting a new era in testing MHD accretion-disk theory or BLR physics.

#### 5. SUMMARY

## ACKNOWLEDGMENTS

We thank the anonymous referee for his/her useful and timely comments that improved the manuscript. M.Y.S. acknowledges support from the National Natural Science Foundation of China (NSFC-11973002). W.N.B. acknowledges support from NSF grant AST-1516784 and NASA ADAP grant 80NSSC18K0878. J.R.T. acknowledges support from NASA grants HST-GO-15260, HST-GO-15650, and 18-2ADAP18-0177, and NSF grant CAREER-1945546. Z.F.Y. was supported in part by the United States National Science Foundation under Grant No. 161553. Y.Q.X. and J.X.W. acknowledge support from the National Natural Science Foundation of China (NSFC-12025303, 11890693, 11421303), the CAS Frontier Science Key Research Program (QYZDJ-SSW-SLH006), and the K.C. Wong Education Foundation. Z.Y.C. acknowledges support from the National Natural Science Foundation of China (NSFC-11873045). J.X.W., W.M.G., Z.Y.C. and Z.X.Z. acknowledge support from the National Natural Science Foundation of China (NSFC-12033006). T.L. acknowledges support from the National Natural Science Foundation of China (NSFC-11822304). Y.H. acknowledges support from NASA grants HST-GO-15650. J.F.W. acknowledges support from National Natural Science Foundation of China (NSFC-U1831205). We thank Prof. Jianfeng Wu for his helpful suggestions.

**Table 1.** The adopted bands to fit the inter-band lag-wavelength relation.

Source name	Adopted bands	Reference band	Reference
NGC4593	UVM2, UVW1, UVB, UVV, 1150 Å, 1350 Å, 1460 Å, 1690 Å, 4745 Å, 5100 Å, 5450 Å, 5600 Å, 6250 Å, 6850 Å, 7450 Å, 8000 Å, 8800 Å, 9350 Å	UVW2	Cackett et al. (2018)
NGC 2617	UVW2, UVM2, UVW1, UVB, g, UVB, r, i, z	5100 Å	Fausnaugh et al. (2018)
MCG+08-11-011	r, i, z	g	Fausnaugh et al. (2018)
NGC 4151	UVM2, UVW1, UVB, UVV	UVW2	Edelson et al. (2017)
Mrk 142	UVM2, UVW1, UVB, g, v, UVV, r, I, z	UVW2	Cackett et al. (2020)
NGC 5548	1158 Å, 1479 Å, 1746 Å, UVW2, UVM2, UVW1, B, UVB, g, V, r, R, I, i, z	1367 Å	Fausnaugh et al. (2016)
Fairall 9	UVM2, UVW1, UVB, UVV, B, g, v, r, i, z <sub>s</sub>	UVW2	Hernández Santisteban et al. (2020)
Ark 120	B, UVW1, UVB, UVV	I	Lobban et al. (2020)
NGC 7469	V	UVW2	Pahari et al. (2020)
Mrk 509	UVM2, UVW1, UVB, UVV	UVW2	Edelson et al. (2019)
PG 2308+098	g, r, i, z	u	Kokubo (2018)
H19 quasars	i	g	Homayouni et al. (2019)
Y20 quasars	r, i, z	g	Yu et al. (2020)

## APPENDIX

## A. ESTIMATING THE TIME LAGS AT 2500 Å

The time-lag measurements of previous studies correspond to various rest-frame wavelengths. Hence, for each source, we fit the function  $\tau = \tau_0((\lambda/\lambda_0)^\beta - 1)$  with  $\beta \equiv 4/3$  (as  $\beta$  cannot be well constrained for most sources) to these time-lag measurements by minimizing the  $\chi^2$  statistic (i.e., with only one free parameter  $\tau_0$ ), where  $\tau$  and  $\lambda$  are the rest-frame time lag and wavelength (the subscript 0 indicates the reference band), respectively. The best-fitting  $\tau_0$  is used to infer  $\tau_{\text{obs}}$  (i.e.,  $\tau_{\text{obs}} = \tau_0(2500 \text{ Å}/\lambda_0)^\beta$ ). Note that the cross correlation and *Javelin* (Zu et al. 2011) are often used to measure the time lags of local AGNs; for more distant luminous AGNs, *Javelin* is often preferred. We adopt the *Javelin* time-lag measurements reported by previous studies to fit the above function; if the *Javelin* time-lag measurements are unavailable, we use the cross-correlation centroids (e.g., NGC 4151) since the two methods are generally consistent with each other (see, e.g., Figure 4 of Fausnaugh et al. 2016). We note that the X-ray bands are excluded when fitting the lag-wavelength function. The *u*-band is also excluded except for the  $z = 0.433$  quasar, PG2308+098 (for this source, the *u*-band is adopted as the reference band and the corresponding rest-frame wavelength is 2478 Å). The adopted bands for each source are listed in Table 1.

## REFERENCES

- Baldwin, J. A. 1977, ApJ, 214, 679  
Cackett, E. M., Chiang, C.-Y., McHardy, I., et al. 2018, ApJ, 857, 53  
Cackett, E. M., Gelbord, J., Li, Y.-R., et al. 2020, ApJ, 896, 1  
Cai, Z.-Y., Wang, J.-X., & Sun, M. 2020, ApJ, 892, 63  
H-H. Chan, J., Millon, M., Bonvin, V., et al. 2020, A&A, 636, A52  
Chelouche, D., Pozo Nuñez, F., & Kaspi, S. 2019, Nature Astronomy, 3, 251  
Cornachione, M. A., Morgan, C. W., Burger, H. R., et al. 2020, ApJ, 905, 7  
Edelson, R., Gelbord, J., Cackett, E., et al. 2017, ApJ, 840, 41  
Edelson, R., Gelbord, J., Cackett, E., et al. 2019, ApJ, 870, 123  
Fausnaugh, M. M., Denney, K. D., Barth, A. J., et al. 2016, ApJ, 821, 56  
Fausnaugh, M. M., Starkey, D. A., Horne, K., et al. 2018, ApJ, 854, 107

- Flaugher, B., Diehl, H. T., Honscheid, K., et al. 2015, *AJ*, 150, 150.
- Ganguly, R., Brotherton, M. S., Cales, S., et al. 2007, *ApJ*, 665, 990.
- Gil-Merino, R., Goicoechea, L. J., Shalyapin, V. N., et al. 2012, *ApJ*, 744, 47
- Hall, P. B., Sarrouh, G. T., & Horne, K. 2018, *ApJ*, 854, 93
- Hernández Santisteban, J. V., Edelson, R., Horne, K., et al. 2020, *MNRAS*, 498, 5399
- Homayouni, Y., Trump, J. R., Grier, C. J., et al. 2019, *ApJ*, 880, 126
- Ivezić, Ž., Kahn, S. M., Tyson, J. A., et al. 2019, *ApJ*, 873, 111
- Jiang, Y.-F., Green, P. J., Greene, J. E., et al. 2017, *ApJ*, 836, 186
- Kammoun, E. S., Papadakis, I. E., & Dovčiak, M. 2021, *MNRAS*
- King, A. R., Pringle, J. E., & Livio, M. 2007, *MNRAS*, 376, 1740
- Kokubo, M. 2018, *PASJ*, 70, 97
- Korista, K. T. & Goad, M. R. 2019, *MNRAS*, 489, 5284
- Krolik, J. H., Horne, K., Kallman, T. R., et al. 1991, *ApJ*, 371, 541
- Laor, A. & Brandt, W. N. 2002, *ApJ*, 569, 641. doi:10.1086/339476
- Laor, A. & Davis, S. W. 2014, *MNRAS*, 438, 3024.
- Lawther, D., Goad, M. R., Korista, K. T., et al. 2018, *MNRAS*, 481, 533.
- Li, Y.-P., Yuan, F., & Dai, X. 2019, *MNRAS*, 483, 2275
- Lidman, C., Tucker, B. E., Davis, T. M., et al. 2020, *MNRAS*, 496, 19.
- Lobban, A. P., Zola, S., Pajdosz-Śmierciak, U., et al. 2020, *MNRAS*, 494, 1165
- MacLeod, C. L., Ivezić, Ž., Kochanek, C. S., et al. 2010, *ApJ*, 721, 1014
- McHardy, I. M., Connolly, S. D., Horne, K., et al. 2018, *MNRAS*, 480, 2881
- Morgan, C. W., Hyer, G. E., Bonvin, V., et al. 2018, *ApJ*, 869, 106
- Mudd, D., Martini, P., Zu, Y., et al. 2018, *ApJ*, 862, 123
- Pahari, M., McHardy, I. M., Vincentelli, F., et al. 2020, *MNRAS*, 494, 4057
- Richards, G. T., Lacy, M., Storrie-Lombardi, L. J., et al. 2006, *ApJS*, 166, 470
- Shakura, N. I., & Sunyaev, R. A. 1973, *A&A*, 24, 337
- Shields, J. C. 2007, *The Central Engine of Active Galactic Nuclei*, 373, 355
- Sun, M., Xue, Y., Brandt, W. N., et al. 2020a, *ApJ*, 891, 178
- Sun, M., Xue, Y., Cai, Z., et al. 2018a, *ApJ*, 857, 86
- Sun, M., Xue, Y., Guo, H., et al. 2020b, *ApJ*, 902, 7
- Sun, M., Xue, Y., Trump, J. R., et al. 2019, *MNRAS*, 482, 2788
- Sun, M., Xue, Y., Wang, J., et al. 2018b, *ApJ*, 866, 74
- Tie, S. S., & Kochanek, C. S. 2018, *MNRAS*, 473, 80
- Yu, Z., Martini, P., Davis, T. M., et al. 2020, *ApJS*, 246, 16
- Zhu, F.-F., Wang, J.-X., Cai, Z.-Y., et al. 2018, *ApJ*, 860, 29
- Zu, Y., Kochanek, C. S., & Peterson, B. M. 2011, *ApJ*, 735, 80. doi:10.1088/0004-637X/735/2/80